Structure of a dehydratase–isomerase from the bacterial pathway for biosynthesis of unsaturated fatty acids: two catalytic activities in one active site

Minsun Leesong[1], Barry S Henderson[2†], James R Gillig[2‡], John M Schwab[2§*] and Janet L Smith[1*]

Background: *Escherichia coli* β-hydroxydecanoyl thiol ester dehydrase (dehydrase) is essential to the biosynthesis of unsaturated fatty acids, by shunting a 10-carbon intermediate from the saturated fatty acid pathway into the unsaturated fatty acid pathway. Dehydrase catalyzes reactions of dehydration and of double-bond isomerization on 10-carbon thiol esters of acyl carrier protein (ACP). The aim of this work is to elucidate mechanisms for the two enzymatic reactions, which occur in an unusual bifunctional active site, and to understand the specificity of the enzyme for substrates with 10-carbon fatty acyl chains.

Results: Crystal structures at 2.0 Å resolution for free dehydrase and for the enzyme modified by its classic, mechanism-based inactivator, 3-decynoyl-*N*-acetylcysteamine, have been determined. Dehydrase is a symmetric dimer with an unusual α+β 'hot dog' fold. Each of the two independent active sites is located between the two subunits of the enzyme, and is a tunnel-shaped pocket completely isolated from the general solvent. Side chains of histidine from one subunit and aspartic acid from the other are the only potentially reactive protein groups in the active site.

Conclusions: A two-base mechanism by which the histidine and aspartic acid together catalyze dehydration and isomerization reactions is consistent with the active-site structure. The unique topology of the protein fold and the identification of the active-site components reveal features of predictive value for another enzyme, FabZ, which may to be the non-specific dehydratase involved in elongation of fatty acyl chains. A positively charged area surrounding the entrance to the active site, which could interact with the negatively charged ACP, was also found.

Addresses: [1]Department of Biological Sciences and [2]Department of Medicinal Chemistry and Pharmacognosy, Purdue University, West Lafayette, IN 47907, USA.

Present addresses: [†]Department of Biology, Massachusetts Institute of Technology, Cambridge, MA 02139, USA, [‡]Lilly Research Laboratories, Eli Lilly and Company, Indianapolis, IN 46285, USA and [§]Food and Drug Administration, HFD-150, 5600 Fishers Lane, Rockville, MD 20857, USA.

*Corresponding authors.

Key words: bifunctional enzyme, crystal structure, dehydratase, fatty acid biosynthesis, isomerase, suicide inhibition

Received: **2 Jan 1996**
Revisions requested: **12 Jan 1996**
Revisions received: **24 Jan 1996**
Accepted: **24 Jan 1996**

Structure 15 March 1996, **4**:253–264

Introduction

Unsaturated fatty acids are indispensable to virtually all life forms. Some important roles include modulation of biological membrane fluidity and serving as precursors to other essential cell components.

Whereas eukaryotes utilize molecular oxygen to desaturate full-length, saturated fatty acids, this route is not available to organisms that live under anaerobic conditions. In certain bacterial systems, an unsaturated intermediate in the biosynthetic pathway of saturated fatty acids is intercepted and shunted into the pathway leading to unsaturated products. In *Escherichia coli*, the enzyme β-hydroxydecanoyl thiol ester dehydrase (dehydrase; EC 4.2.1.60) is responsible for this key step [1]. Dehydrase catalyzes two reactions on fatty acid thiol esters of acyl carrier protein (ACP): the dehydration of (*R*)-3-hydroxydecanoyl-ACP to (*E*)-2-decenoyl-ACP, a reaction that also occurs in the elongation of saturated fatty acids; and the isomerization of (*E*)-2-decenoyl-ACP to (*Z*)-3-decenoyl-ACP (Fig. 1a). (*E*)-2-decenoyl-ACP can be reduced to decanoyl-ACP, which is elongated to the usual saturated fatty acids; in contrast, the *cis* (*Z*) double bond of (*Z*)-3-decenoyl-ACP is retained through the further cycles of fatty-acid elongation. The isomerization catalyzed by dehydrase is an allylic rearrangement [2], which is a relatively simple, single-substrate reaction. Both the dehydration and isomerization reactions seem to occur in the same active site [3,4].

The substrate specificity of dehydrase is notable [1,5,6]. It is highly specific for unbranched 10-carbon substrates, and this accounts for the fact that *E. coli* contains a very limited constellation of unsaturated fatty acids, all with one *cis* double bond six carbons from the terminal methyl group. The activity of dehydrase on branched fatty acid thiol esters or on 8-carbon or 12-carbon intermediates is negligible. On the other hand, thiol esters of ACP are not

Figure 1

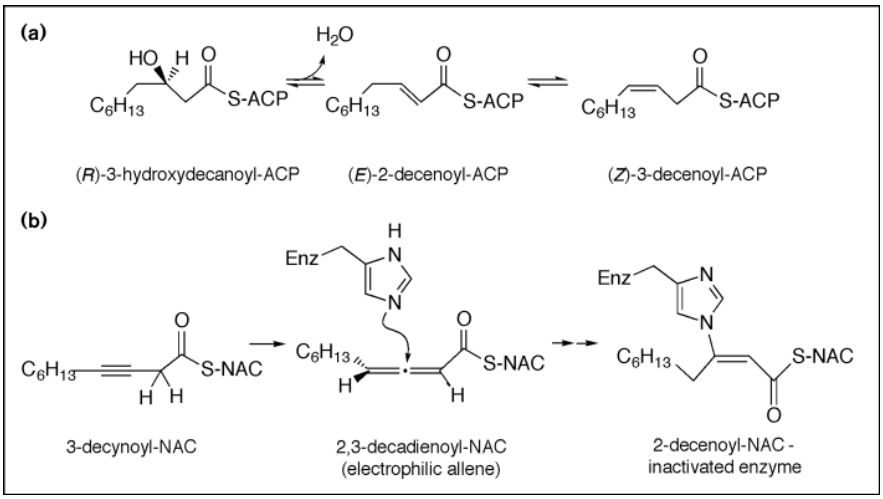

Catalytic reactions of dehydrase. **(a)** Biological reactions of dehydration and isomerization. **(b)** Inactivation of dehydrase by the mechanism-based inactivator 3-decenoyl-NAC. The first product of inactivation is the 3,4-unsaturated adduct, but this slowly isomerizes to the 2,3-unsaturated form [11]. The double bond configuration has been shown by the present study.

strictly required, as dehydrase also turns over non-protein substrates such as thiol esters of *N*-acetylcysteamine (NAC) or of pantetheine, the ACP prosthetic group.

There is a paucity of structural information on enzymes of fatty-acid biosynthesis due to difficulties in studying the multienzyme complexes or polyproteins of most fatty-acid synthetases. However, the structures of two enoyl ACP reductases have been reported recently [7,8]. Fatty-acid elongation with acetyl-CoA as a two-carbon building block proceeds by iteration of four chemical reactions: condensation, ketone reduction, dehydration and double-bond reduction. Enoyl ACP reductase catalyzes the double-bond reduction step. Dehydrase and enoyl ACP reductase are unrelated enzymes, except for the similarity of their substrates. Comparison of their binding modes for fatty acyl chains may reveal features essential to the 10-carbon specificity of dehydrase and the requisite lack of specificity of enoyl ACP reductase and other enzymes of fatty-acid elongation.

Dehydrase is a soluble homodimer of a 171 amino-acid polypeptide [9,10] with two active sites per dimer [3,11,12]. No metal ions or other cofactors are associated with its function, and no cooperativity has been detected. Thus, dehydrase qualifies as a non-metal dehydratase; structures of this group are less well characterized than are those of dehydratases that employ metal ions. The structure of only one other non-metal dehydratase has been reported [13]. Scytalone dehydratase does not appear to be related to the dehydrase of this work, but elements of the catalytic site may nonetheless prove similar.

The primary structure of dehydrase has been derived from the nucleotide sequence of *fabA*, the gene for dehydrase [9,10]. Dehydrase shares amino-acid sequence similarity with only one other protein, FabZ, whose structure and function are less well studied. On the basis of sequence similarity to dehydrase, Raetz and co-workers gave the name *fabZ* to an open reading frame they discovered among *E. coli* genes for lipid A synthesis [14]; they then expressed and studied the FabZ protein. Their observation of a dehydratase activity for FabZ on hydroxymyristoyl ACP showed that dehydrase and FabZ indeed have similar catalytic activities [15]. This led to the hypothesis that FabZ may be the previously unidentified dehydratase of fatty-acid elongation in *E. coli*.

Dehydrase is of historic importance in the field of enzymology because it was the first enzyme for which mechanism-based, 'suicide' inactivation was recognized [3,16]. In this process, dehydrase catalyzes a propargylic rearrangement of the acetylenic substrate analog 3-decynoyl-NAC, analogous to the allylic rearrangement of the (*Z*)-3-decenoyl thiol ester substrate, creating an electrophilic allene, which then alkylates His70 and inactivates the enzyme (Fig. 1b). Until the present work, the identities of residues other than His70 at the active site of dehydrase were uncertain.

Both reactions catalyzed by dehydrase require deprotonation of a relatively non-acidic substrate without the help of a metal ion cofactor. The deprotonation at C-2 of the substrate has been shown to be the rate-determining step in dehydration [17] and in the mechanism-based transformation of 3-decynoyl-NAC into the reactive allene [18]. Questions remain as to the nature of groups other than His70 that participate in catalysis. Because a weak base alone is not expected to deprotonate the relatively non-acidic substrates efficiently, a hydrogen-bond donor or source of positive charge is expected to stabilize the development of negative charge in the deprotonated species [19–21].

Figure 2

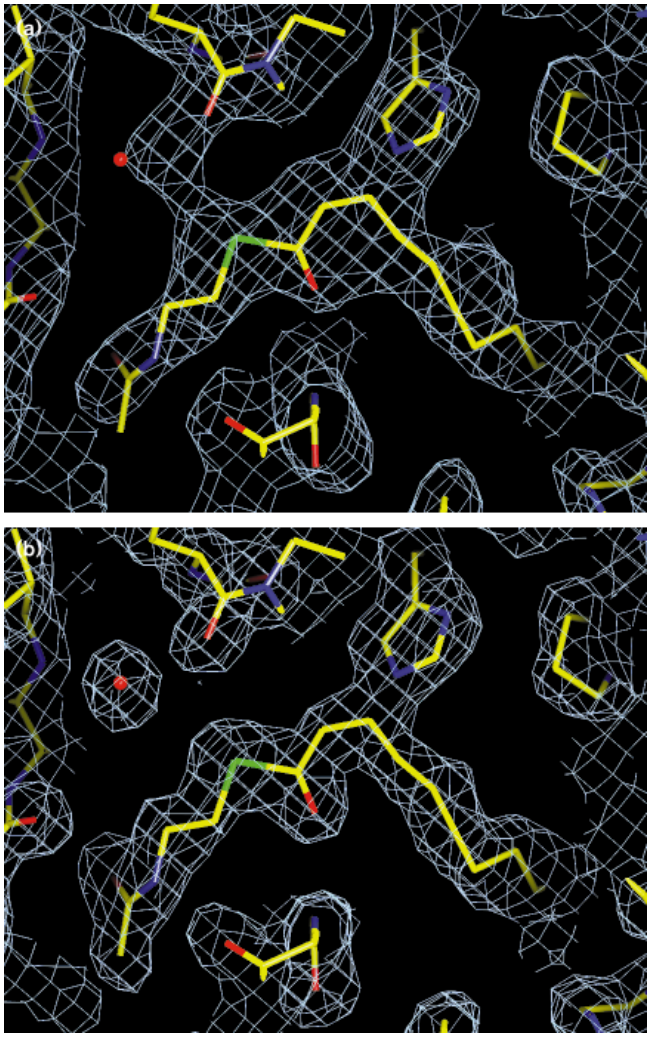

Electron density in the area of the bound inactivator. **(a)** Phase-refined experimental map at 2.5 Å with final model. **(b)** Final $2F_o–F_c$ map at 2.0 Å with final model. Contours for both pictures are drawn at 1.0σ.

X-ray crystal structures at 2.0 Å resolution of dehydrase in a covalent complex with 3-decenoyl-NAC and of the free (native) enzyme are reported here, along with their implications for the catalytic mechanism and substrate specificity.

Results and discussion

Quality of the crystal structures

The electron density for the inactivated structure is continuous and well defined. Three residues, in the N-terminus and the loop formed by residues 134 to 138, have weak density in the structure of the free enzyme. There are no residues in disallowed regions of the Ramachandran plot of either model. Examples of the initial and final electron-density maps are shown in Figure 2. Some indicators of model quality are listed in Table 1.

Table 1

Model statistics.

Enzyme	Inactivated	Free
Data range	7.0–2.0 Å	7.0–2.0 Å
R-factor (F>1σ)	16.3%	18.3%
No. of reflections (F>1σ)	21 941	20 804
R-free (F>1σ)	21.4%	24.3%
R-factor (all data)	16.5%	19.3%
No. of reflections (all data)	22 030	21 621
Rmsd between subunit Cα positions	0.22 Å	0.27 Å
Rmsd bonds	0.010 Å	0.010 Å
Rmsd angles	1.65°	1.63°
No. of protein atoms	2650	2650
No. of water molecules	288	163
Mean protein B-factor	19.2 Å^2	33.0 Å^2
Rmsd protein B-factor between bonded atoms	2.9 Å^2	2.9 Å^2

The protein fold

The dehydrase dimer consists of two identical subunits that make up one compact domain due to extensive hydrophobic and hydrogen-bonding contacts between subunits (Fig. 3). The dimensions of the dimer are approximately 60×40×40 Å. The 171-residue subunit has a mixed α+β 'hot dog' fold. A seven-stranded antiparallel β-sheet 'bun' wraps around a hydrophobic five-turn α-helical 'sausage'. The monomers are joined in a continuous 14-stranded antiparallel β sheet to form the dimer. The view of the hot dog along the sausage axis shows a three-layer segregation of secondary structural elements: a curved β-sheet layer, the central α-helical layer, and a layer consisting largely of loops covering the helix, analogous to condiments on the hot dog.

The topology of the monomer is shown in Figure 4. As far as we can determine, this topology has not been observed in any other proteins. The seven-stranded β sheet forms a highly curved surface. Most of the curvature is created by eight β bulges in each subunit. Four of these, in β4, β5 and β7, are aligned with the central helix and create a crease across the center of the β sheet. The long non-polar central helix (α3) packs against the hydrophobic concave surface of the β sheet. At first glance, aspects of the structure are reminiscent of the class II MHC peptide-binding domains [22] and the dimer capsid protein of bacteriophage MS2 [23]: there is a prominent β sheet across the dimer axis and a pair of helices is located on one face of that sheet. However, dehydrase is fundamentally different from these structures. The helices lie on the concave inner surface of the β sheet in dehydrase, and on the convex outer surfaces of the curved β sheets in MHC II and MS2.

The central helix of dehydrase (α3, residues 79–97) is unusual in that it has the same length and hydrophobicity that characterizes the membrane-spanning anchors of some

Figure 3

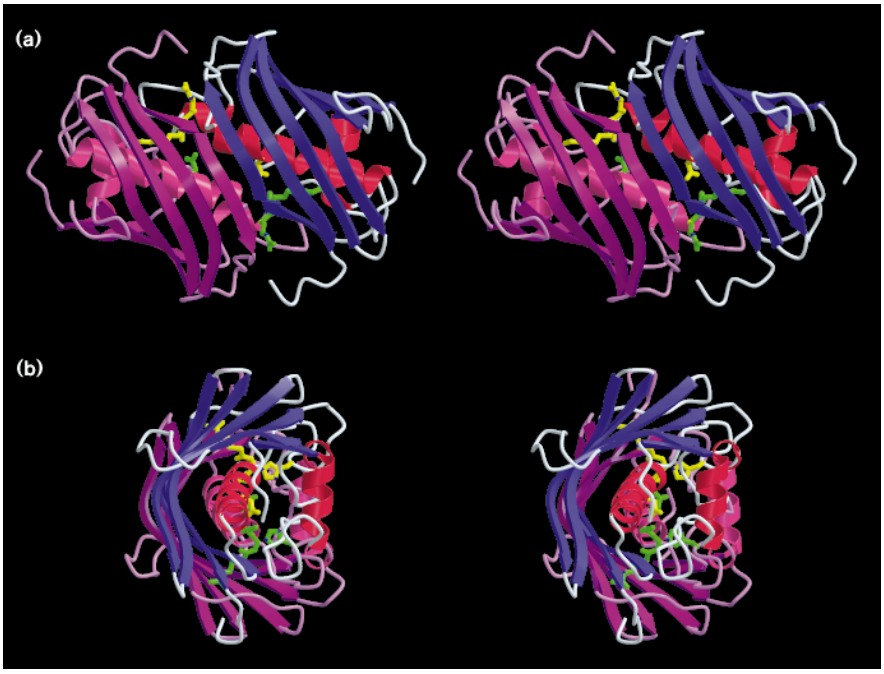

Stereo ribbon diagrams of the dimer of dehydrase. The main-chain trace of one subunit is shown with purple β strands, red helices, and white loops. The side chains of His70 and Asp84, along with the inactivator covalently attached to His70 of this subunit, are shown in yellow. The second subunit of the dimer is shown in magenta, with the side chains and inactivator shown in green. **(a)** View along the dyad axis of the dimer. **(b)** View perpendicular to the dyad, approximately along the axes of the central helices.

membrane proteins. It is virtually buried within the protein, between the β sheet and the loop layer of the polypeptide fold, and has only 10 $Å^2$ of solvent-accessible surface area. Only two of the 19 residues that make up the central helix are polar, and these face the active site. Another example of an extremely hydrophobic helix in a soluble protein was reported recently in HMG-CoA reductase [24].

The crystallographic asymmetric unit contains one dehydrase dimer. Where relevant, amino-acid residues are labelled A or B to refer specifically to one of the two subunits in the asymmetric unit of the crystals. In part of the discussion in which reference to the crystal lattice is irrelevant, primed and unprimed labels are used.

Conflicting evidence for an intrasubunit disulfide bridge has been reported [2,3,25]. An intrasubunit bridge between Cys69 and Cys80, the only cysteine residues in the polypeptide, would require substantial rearrangement of the protein structure. With appropriate side-chain rotations, Cys80A and Cys80B are close enough to form an intersubunit disulfide bridge; however, they are reduced in both crystal structures. The side chains of Cys69A and Cys69B, which are located on the surface of the enzyme, were modified by ethyl mercury phosphate in one of the heavy atom derivatives of crystals of inactivated dehydrase, attesting to their greater reactivity in the crystalline enzyme.

Seven side chains and two peptides of the dimer each have two conformations in the inactivated enzyme. Conformational flexibility of the 109A-110A and 109B-110B peptides, which are hydrogen bonded to one another at the molecular twofold, is caused by β bulges at these residues. Alternative conformers are related by 'flipping' the peptides to reverse the orientation of the amide and carbonyl groups. Conformational flexibility is thus coupled, and either of the mutually compatible A-B conformer pairs break the molecular dyad symmetry. Four of the side chains with dual conformations are on the protein surface (Arg4A, Gln24A, Arg127A and Leu148B), and three are in the hydrophobic core (Met36A, Met36B and Leu83B). Dual conformers also occur for the same residues and peptides in the free enzyme structure, but were more difficult to detect, due to the higher temperature factor of the free enzyme model.

The structures of the inactivated and free enzymes are virtually identical, having a root mean square (rms) deviation in Cα positions of 0.33 Å after superposition. The largest difference is at the C terminus of the polypeptide where the side chain of the terminal Phe171 closes the entrance to the active site in the free enzyme but not in the inactivated enzyme. The large difference (37.8%) in structure amplitudes, between crystals of the two forms of the enzyme, is due to slightly different orientations (2.7°) of the dimers with respect to the crystal axes and to the inactivator itself. It is not due to structural differences between forms of the enzyme.

The active site and catalytic mechanism

The active site of dehydrase is identified by the location of the catalytic residue His70 and by the binding site for the inactivator molecule in the structure of the inactivated

Figure 4

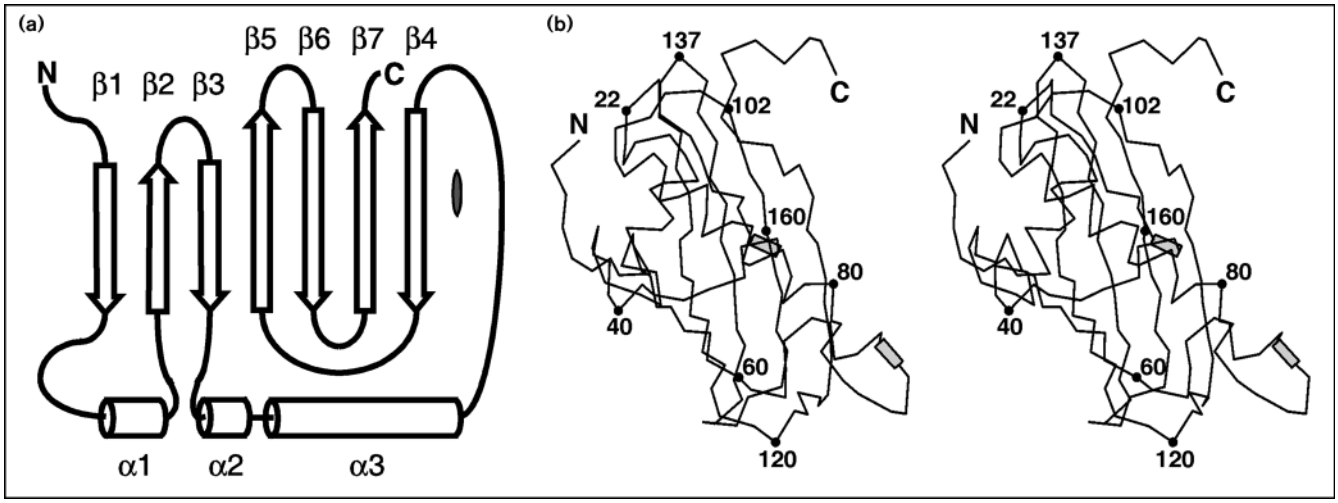

Structure of the dehydrase monomer. **(a)** Topology of the polypeptide fold. β strands are represented as arrows labelled β1–β7. The helices are represented as cylinders labelled α1–α3 (α2 is a 3_{10}-helix). The dyad axis is adjacent to β4. **(b)** Stereo view of the Cα trace of the purple subunit of Figure 3, viewed along the dyad axis. The positions of the two non-proline *cis* peptides are shown as shaded boxes.

enzyme (Fig. 5). The two active sites of the dimer are symmetrically displaced about the molecular dyad, and are separated by ~20 Å. The active sites are identical, to within experimental error, and appear to be completely independent of one another, in accord with the reported lack of cooperativity in substrate binding or catalysis for the two active sites of the dimer [3,11,12]. Unexpectedly, each active site is situated at the subunit interface and is formed in equal part by the two subunits. This, and the extensive hydrophobic contact between subunits, is consistent with the fact that efforts to observe enzyme activity in isolated subunits were unsuccessful [26].

The design of the active site exploits the unusual features of the dehydrase fold so that catalysis with the hydrophobic substrate occurs far from the bulk solvent. The substrate/inactivator-binding site is a tunnel-shaped pocket, 20 Å long and 6 Å wide, reflective of the shape of the linear substrate. The pocket resembles a worm hole that begins at the subunit interface, between strands β4 and β4′, and burrows into the hydrophobic core of the protein between the central helix and inner surface of the β sheet. The innermost half of the worm hole is hydrophobic and is formed predominantly by residues of one subunit. Residues from the other subunit form the outermost, polar half of the worm hole. In the structure of the inactivated enzyme, the aliphatic tail of the inactivator fills the hydrophobic half of the binding pocket, and the *N*-acetylcysteamine moiety fills the polar half. Binding of the inactivator plugs the worm hole, so that the catalytic site is highly sequestered from bulk solvent. Less than 0.5% (2.3 Å^2) of the total surface area of the bound inactivator is solvent accessible. In the structure of the free enzyme, the tunnel is filled with solvent molecules, and the entrance is plugged by the side chain of the C-terminal residue Phe171, so that the active site is an isolated cavity.

Residues of potential catalytic importance come from both subunits (Fig. 5). His70 is situated halfway along the binding tunnel and belongs to the subunit that forms the polar half of the binding site. It is covalently modified at Nε2 by the inactivator. The space immediately surrounding His70 is generally non-polar, with the notable exception of Asp84′ and a water molecule bound to Asp84′ and to Cys80, at the N terminus of the central helix (α3). Asp84′, which was not anticipated to be a catalytic residue, is in direct contact with the C-3/C-4 region of the inactivator. Since His70 was identified as the site of covalent modification by 3-decynoyl NAC [18], studies of the mechanism of dehydrase have focused on this residue. Modification of His70 at Nε2 was demonstrated by ^{15}N NMR [7]. In the same study, His70 was shown to be unprotonated in the free enzyme at pH values as low as 5, consistent with the isolation of the active site from bulk solvent. This NMR result, in combination with the crystal structure, also demonstrates that the free enzyme does not include an imidazolium–carboxylate ion pair between His70 and Asp84′.

In most respects, the active sites of the inactivated and free enzymes are identical to within experimental error (Fig. 5c). This identity includes the rare non-proline *cis* peptide between His70 and Phe71. Another *cis* peptide bond, between Pro31 and Asn32, is part of a loop near the binding pocket for the acyl chain and also occurs in both the inactivated and free enzymes (the locations can be seen in Fig. 4b). Few non-proline *cis* peptides have been

Figure 5

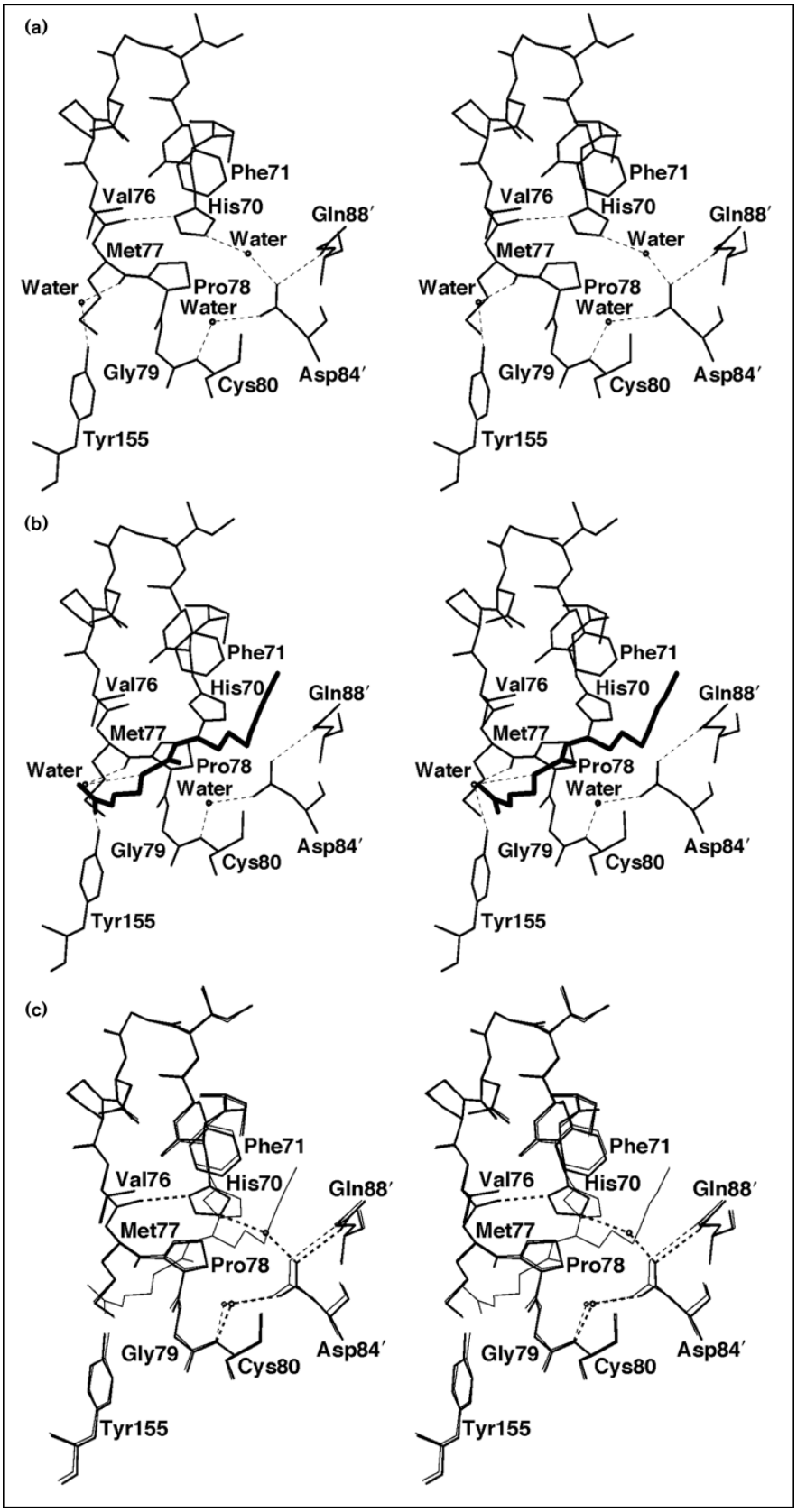

Stereo view of residues in the catalytic region of the substrate-binding site. Only water molecules in hydrogen-bonding contact with the catalytically important region of the pocket are shown here. Dashed lines are hydrogen bonds. **(a)** Active site of the free enzyme. **(b)** Active site of the inactivated enzyme. The inactivator is bonded to Nε2 of His70, and the water molecule between His70 and Asp84′ of the free enzyme is not present. **(c)** Superposition of active sites of inactivated and free enzymes. Overlay is based on a superposition of the Cα atoms of residues 69–80, which results in an rms deviation of 0.17 Å.

Figure 6

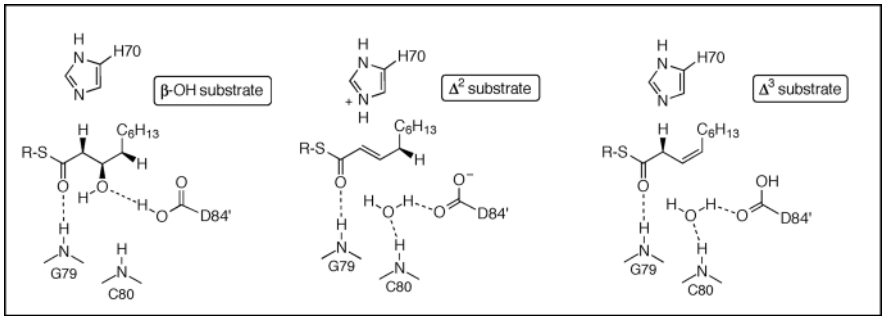

Proposed binding mode for substrates. Dehydrase interconverts the 2/3-*trans* unsaturated (Δ^2) and either the 3-hydroxy (β-OH) or the 3,4-*cis* unsaturated (Δ^3) decanoyl thiol esters (Fig. 1a). The proposed substrate complexes, shown here in schematic form, exploit the proximal side chains of His70 and Asp84′, which may carry out both catalytic conversions occurring in the same active site. This scheme is consistent with the established stereochemistry of the reactions [4]. Peptide dipoles from Gly79 and Cys80 at the N terminus of the central α helix (α3) may provide stabilization to the presumed enol/enolate intermediate and to the leaving hydroxyl group. Hydrogen bonds are depicted as dashed lines.

observed in highly refined crystal structures of proteins, and nearly all are associated with active sites [27], as is the case for the 70–71 peptide of dehydrase.

The most notable difference between the inactivator-attached and free states of the enzyme is the orientation of the imidazole ring of His70. His70 in the free enzyme donates a proton in a hydrogen bond from Nδ1 to the backbone carbonyl of Val76 (Fig. 5a), as previously observed by ^{15}N NMR [7]. This is consistent with a catalytic role for histidine, because it results in a basic lone pair of electrons on Nϵ2. The hydrogen bond of Nδ1 also positions the imidazole ring rather precisely. Thus, we infer that His70 is in the correct tautomeric state and optimal orientation for catalysis in the free enzyme. This situation does not prevail in the inactivated enzyme, where covalent attachment of the inactivator disrupts the protonation state and conformation of His70. The covalent bond between the inactivator and Nϵ2 of His70 results in loss of a proton by Nδ1 (Fig. 1b), which is then unable to form a hydrogen bond with the carbonyl of Val76. The net result is that the imidazole ring is flipped by ~180° and moved away from Val76 (Fig. 5c). The Nϵ2 atom occupies the same position in both structures. Because the structure of His70 in the inactivated enzyme seems to be a direct result of the covalent attachment of the inactivator, we assume that the hydrogen-bonded configuration and orientation of His70 in the free enzyme are relevant to the situation where substrates are non-covalently bound.

The flip of the His70 imidazole may also be related to an unexpected double-bond configuration for the inactivator. The double bond in the 2-decenoyl thiol ester substrate/product of dehydrase is in the *trans* (*E*) configuration. This was the configuration expected for the corresponding double bond in the inactivator moiety of the inactivated enzyme. However, the inactivator, as generated by the enzyme from the acetylenic starting material and covalently attached to His70, has an (*E*)-2 double bond (*cis* with respect to the carbon chain of the inactivator; Fig. 5b). The conformation of the inactivator and its double-bond configuration can be stated with confidence because of the 2.0 Å resolution of the electron density maps and the unbiased method used to model the inactivator into its density (see the Materials and methods section). The observed *cis* double bond indicates that some important details of substrate/product binding in the active site are not mimicked by the binding of the inactivator.

The active sites of both the inactivated and free enzymes include water molecules. In the inactivated enzyme, one water molecule is hydrogen bonded to the peptide nitrogen of Cys80 and to a carboxyl oxygen of Asp84′ (Fig. 5b), and another water molecule is hydrogen bonded to a Tyr155 hydroxyl group and to the sulfur atom in the inactivator. The two water molecules occupy the same positions in the free enzyme, which has an additional water bridge between the side chains of Asp84′ and His70 (Fig. 5a). Two of these waters may participate in catalysis. Five additional water molecules are in the substrate-binding pocket of the free enzyme, all hydrogen bonded to either the protein or to each other.

A two-base mechanism is suggested as an attractive alternative to the one-base mechanism [2,4,28,29] that has, for a long time, been presumed for dehydrase. This proposal is based on the structure of the active site, with His70 and Asp84′ centered in the largely hydrophobic substrate-binding pocket. Figure 6 illustrates how His70 and Asp84′ might be positioned with respect to the 3-hydroxy, the 2,3-*trans* unsaturated and the 3,4-*cis* unsaturated substrates and products of dehydrase (Fig. 1a), in such a way that both amino acid side chains might participate directly in substrate protonation and deprotonation. It is also proposed that one of the bound water molecules is the stored water of hydration. This water is hydrogen bonded between Asp84′ and the peptide nitrogen of Cys80 in the structures of both the free and the inactivated enzymes. This water/hydroxyl and the reaction intermediate enol/enolate [19] may be stabilized by the positive dipole at the N terminus of the central α helix via hydrogen bonds to NHs of Cys80 and Gly79, respectively. A more detailed discussion of possible reaction mechanisms is being published separately.

Figure 7

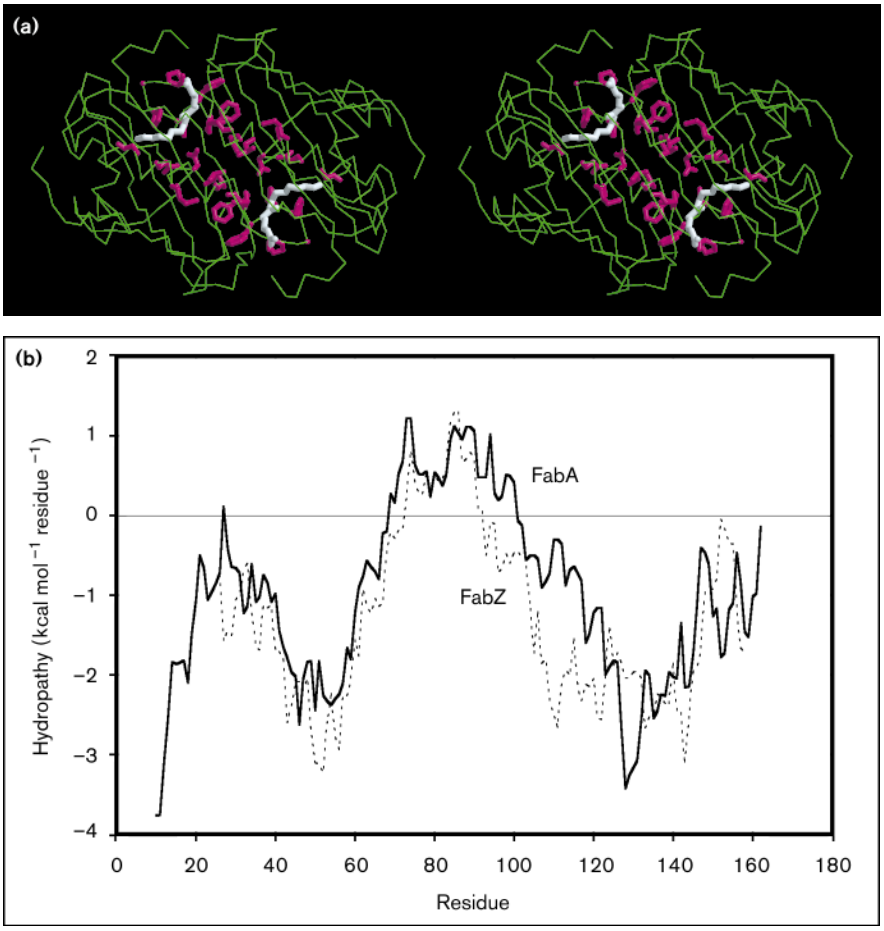

Similarity of dehydrase and FabZ. **(a)** Residues conserved in the sequence alignment of dehydrase and FabZ. In the same view as Figure 3a, the Cα trace of the dimer is in green. Identical residues within the region of significant sequence similarity (residues 60–90 of dehydrase) are shown in magenta. The bound inactivators are shown in white to locate the active sites. The conserved residues are clustered around the active sites and along the central helices. Conserved residues (also shown in Fig. 5) are His70, Phe71, Gly73, Pro75, Pro78, Gly79 and Gln88. **(b)** Hydrophobicity profiles of dehydrase (FabA) and FabZ. Hydropathy is calculated based on the Engelman *et al.* polarity scale [50] with a window size of 19 residues. The 171-residue dehydrase and the 150-residue FabZ are aligned with residues 60–90 of dehydrase corresponding to residues 44–74 of FabZ.

Substrate specificity

The extreme specificity of dehydrase for substrates with 10-carbon aliphatic chains can be explained by structural features of the substrate-binding pocket. The pocket is not deep enough for extended 12-carbon chains nor wide enough for folded or branched chains. The situation with respect to short molecules is less clear. However, the near identity of filled and empty binding pockets indicates that a substrate-induced rearrangement of the protein structure is not the basis for the 10-carbon specificity.

Selectivity against short substrates may be provided by the combined effects of a closed inner end of the binding pocket and a lack of enzyme specificity for the polar end of the substrate. That is, substrate-like molecules with eight or fewer carbons in the aliphatic chain may bind too far into the pocket to effect catalysis. The specificity and structure of enoyl ACP reductase [7,8] lend support to this idea. Enoyl ACP reductase does not have a closed-end binding pocket, but has on its surface a hydrophobic cleft for acyl-chain binding. Thus, the open binding site of enoyl ACP reductase may be associated with lack of specificity for length of the acyl chain, whereas the 10-carbon specificity of dehydrase is a feature of the closed pocket.

Acyl carrier protein and dehydrase

The natural fatty acyl substrate for dehydrase is covalently attached to ACP by a phosphopantetheine prosthetic group. The fatty acyl chain and part of this arm-like prosthetic group bind inside the enzyme, and approximately half of the prosthetic group is assumed to protrude from the active-site tunnel at the dimer interface. Although the requirement of dehydrase for ACP-thiol ester substrates is not as stringent as for other enzymes of fatty acid biosynthesis in *E. coli* [1], the K_m of dehydrase is more than 100-fold lower [30,31], and the turnover rate is six times greater with the ACP substrate than with the NAC thiol ester substrate [5]. ACP substrates also show a significantly different product distribution than that shown by NAC substrates [31]. ACP is expected to interact with dehydrase near the entrance to the active site. The surface potentials for dehydrase and ACP [32,33] reveal regions of electrostatic complementarity. The positively charged patch around the entrance of the substrate-binding site of dehydrase is large enough to

span the diameter of the negatively charged surface of ACP surrounding the pantetheine attachment site.

Relationship of dehydrase to other proteins

Apart from this work, scytalone dehydratase is the only metal-free dehydratase of known structure [13]. The folds of dehydrase and scytalone dehydratase are unrelated, although both are α+β proteins. The active site of scytalone dehydratase includes two basic residues, both histidine, that are proposed to serve as bases in the reaction mechanism, and also includes a proposed 'storage site' for water between the histidines. As in dehydrase, the active site is sequestered from bulk solvent. Hydrogen bonds to water and to protein side chains are available to stabilize the expected enol/enolate intermediate in the reaction pathway, but no α-helix dipole is involved. Thus, while the dehydration reactions catalyzed by dehydrase and by scytalone dehydratase are similar, structural features of the enzymes, both in aggregate and in detail, appear unrelated.

FabZ, whose gene was discovered in conjunction with those involved in lipid A biosynthesis [14], was postulated to be related to dehydrase on the basis of sequence similarity in the region of His70. It was also shown that FabZ could catalyze dehydration reactions, and therefore it was proposed to be the non-specific dehydratase of saturated fatty acyl chain elongation [15]. For the following reasons, we expect FabZ and dehydrase to have a common overall fold. First, the proteins have similar catalytic activity; both catalyze dehydration of hydroxyacyl ACP substrates. Second, a region of significant sequence identity clusters in the functionally and structurally important region of dehydrase; the conserved residues are at the active site and in the core helix of dehydrase (Fig. 7a). There is 65% identity between residues 60 and 90, which accounts for most of the 23% overall identity. Finally, hydrophobicity profiles of dehydrase and FabZ are very similar, most strikingly in the region corresponding to the unusual, hydrophobic, central helix of dehydrase (Fig. 7b). None of these arguments alone is convincing evidence for a common structure, but taken together they make a compelling case. The core of the dehydrase structure is expected to be conserved in FabZ. This conservation should include the fold topology, the central buried helix, the dimerization via a continuous β sheet, the location of the active site between subunits, and the detailed structure of the active site.

The major functional difference between FabZ and dehydrase is that FabZ apparently lacks the ability to catalyze the isomerization reaction. This may be controlled by the replacement of Asp84 in dehydrase with glutamate in FabZ, this being the only residue facing the active site that differs in the two enzymes. Additionally, FabZ is not specific for 10-carbon substrates. This is easily rationalized in terms of the three-dimensional structure of dehydrase. The acyl-chain-binding pocket of dehydrase is formed primarily by residues from the C terminus of the central helix, together with a loop near the N terminus of the polypeptide chain (residues 26–29). Residues 1–25 also contribute to the innermost end of the binding pocket. Hydrophobicity profiles of dehydrase and FabZ (Fig. 7b) indicate that both the shorter N terminus of FabZ and the C terminus of the presumed central helix are more hydrophilic than are the analogous segments of dehydrase. Thus, the binding pocket of dehydrase may be an open-ended tunnel in FabZ, accounting for the ability of FabZ to dehydrate (*R*)-3-hydroxymyristoyl ACP, which is four carbons longer than the substrates for dehydrase [15].

Biological implications

β-hydroxydecanoyl thiol ester dehydrase (dehydrase) is the key enzyme in the synthesis of unsaturated fatty acids in *Escherichia coli,* catalyzing reactions of dehydration and isomerization. It is likely to play a similar role in many other bacteria. This soluble enzyme is also known for its classic susceptibility to mechanism-based inactivation by a synthetic substrate analog. In this report, 2.0 Å resolution structures of dehydrase in its free and inactivated forms reveal the catalytic components of the bifunctional active site.

The topology of the polypeptide is unlike the β barrels of fatty acid binding proteins or indeed any other known fold, with the arrangement of secondary structural elements resembling a 'hot dog'. FabZ, an enzyme postulated to be the dehydratase involved in fatty acyl chain elongation, is predicted also to have this fold. This assumption is based on significant sequence identity with dehydrase in the active-site region and on similarity of hydropathy profiles.

As is the case for other *E. coli* enzymes involved in fatty acid biosynthesis, the natural substrates of dehydrase are covalently attached to acyl-carrier protein (ACP). Surrounding the entrance to the active site of dehydrase is a large positively charged surface, which may interact with the acidic surface of ACP.

Dehydrase catalyzes dehydration and isomerization reactions by a mechanism that does not involve metals or other cofactors, unlike the majority of enzymes that carry out dehydration reactions. The catalytic site is completely isolated from solvent, and is hydrophobic except for a histidine and an aspartic acid, which together are proposed to catalyze both reactions.

Materials and methods

The structure of the inactivator-bound enzyme was determined by multiple isomorphous replacement (MIR) to 2.0 Å resolution. As the inactivated enzyme is of the same crystal form as the free enzyme, this structure was the direct basis of a phasing model to obtain the 2.0 Å structure of the free enzyme.

Crystallization and data collection

Recombinant *E. coli* dehydrase was produced in a high-level expression system and purified according to published protocol [9,10,34]. Purified protein was concentrated to ~10 mg ml^{-1} in a Millipore microfuge concentrator and then filtered through a 0.22 μm Millipore microfuge filter. To inactivate the enzyme, 20 μl of 3.7 mM 3-decynoyl-NAC in acetone was added to 0.50 ml of 2.5 mg ml^{-1} protein to give a 1.5:1 molar ratio of inactivator to protein subunit and an acetone concentration of <2% (v/v). In control experiments, this concentration of acetone was shown to have no detectable effect on enzyme activity. The solution was incubated on ice for 1 h, the time required for 99.7% inactivation of the enzyme as judged by spectrophotometric assay [35]. Inactivated enzyme was then concentrated and filtered as described above.

Crystals of dehydrase were grown according to published conditions [36], with the following variations. The success rate of crystallization was improved by microseeding (K Bennett, M Leesong, A Sharma, JR Gillig, JM Schwab and JL Smith. Crystallization by seeding of β-hydroxydecanoyl thiol ester dehydrase. Abstracts of the American Crystallographic Association Meeting 1991,Vol. 19, p. 74), which ensured reliable growth of small crystals of dimensions less than 0.1 mm. The small crystals were transferred as macroseeds to fresh growth solutions. Crystals typically grew to sizes of 0.3–0.7 mm in each dimension. Crystal growth for inactivated and free dehydrase was complete in one to two weeks by hanging drop vapor diffusion at 21°C. The seeded drop was a mixture of equal volumes of protein solution (10 mg ml^{-1} dehydrase in 10 mM phosphate buffer of pH 7.5) and well solution (18–20% polyethylene glycol (PEG) 8000, 50 mM sodium citrate pH 5.0). The crystals could be stabilized in the well solution with up to 24% PEG 8000. The optimal precipitant (PEG 8000) concentration for growing crystals of the inactivated enzyme from a macroseed was 18%, whereas it was 20% for the free enzyme. The free dehydrase crystals tended to dissolve if not stabilized within one day after they were fully grown. Intensity comparisons, from precession photography at room temperature, of inactivated and free dehydrase crystals showed that the two crystals were only approximately isomorphous. They are of spacegroup $P2_12_12_1$ with two monomers per asymmetric unit and 47% solvent by volume. The cell constants of the two forms, however, do not differ greatly (for the inactivated enzyme a=68.0 Å, b=86.8 Å, c=60.3 Å; for the free enzyme a=68.5 Å, b=86.9 Å, c=60.5 Å).

Data for inactivated dehydrase and its isomorphous derivatives (Table 2) were collected with a Siemens area detector diffractometer on an Elliot GX20 rotating anode operating at 35 kV, 40 mA to produce graphite monochromated CuKα X-radiation. From crystals cooled to 4°, data were collected as 0.1° frames at a crystal-to-detector distance of 100 mm. Data were processed with the program XDS, and scaled and merged with XSCALE [37]. The derivative data were internally scaled with ROTAVATA and AGROVATA in the CCP4 suite of programs [38]. To improve detection of the anomalous signal from the heavy atoms in derivative crystals, the orthogonal cell axes of the crystals were aligned with those of the detector for simultaneous recording of Bijvoet pairs.

Data for free dehydrase (Table 2) were collected from a Rigaku generator producing CuKα X-radiation operating at 50 kV, 100 mA with focusing mirrors. These data were collected at room temperature (21°C) as 0.8° frames on an R-AXIS imaging plate scanning system at a crystal-to-detector distance of 100 mm. Data were processed with DENZO and scaled with SCALEPACK [39].

Phase determination

Two heavy-atom derivatives of the inactivated dehydrase crystals were obtained by soaking (Table 3). The heavy-atom sites for each derivative were located by analysis of isomorphous and anomalous difference Patterson maps, which revealed consistent peak positions. Anomalous scattering data from both derivatives were included in the phase calculation and were also used to determine the correct enantiomorph. Cross-difference Fouriers, constructed with phases calculated from the sites of one derivative, with and without the anomalous data, yielded conclusive differences in heavy-atom peak heights for the other derivative. Heavy-atom parameters (Table 3) were refined using the programs HEAVY [40] and MLPHARE [41]. An MIR map was calculated at 2.5 Å resolution, where the phasing power was greater than 1.0 for both derivatives.

Table 2

Diffraction data and phasing.

	Inactivated native	Inactivated Pt	Inactivated Hg	Free enzyme
Temperature (°C)	4	4	4	21
No. of crystals	3	1	1	1
d_{min} (Å)	2.0	2.2	2.2	2.0
No. of unique refl.	26 075	11 859	11 809	23 461
Redundancy	3.3	2.3	2.3	2.7
Completeness (%)	97	70	70	93
R_{sym} (%)*	4.8	3.9	3.9	6.3
R_{iso} (%)†	–	17.6	10.2	–
Phasing power‡§				
Acentric	–	1.6	1.0	–
Centric	–	1.2	0.9	–
Figure of merit§				
Acentric		0.545		
Centric		0.724		

*$R_{sym}=(\Sigma|I_{hi}-\langle I_h\rangle|)/\Sigma I_{hi}$. †$R_{iso}=(\Sigma||F_{h,native}|-|F_{h,derivative}||)/\Sigma|F_{h,native}|$. ‡Phasing power=$\langle|F_H|\rangle/\langle$lack of closure$\rangle$. §Calculated to 2.5 Å.

MIR phases were refined by molecular averaging and solvent flattening to improve the interpretability of the map. The orientation and position of the local dimer axis were found through calculation of the self-rotation function with the program GLRF [42] and geometric analysis of the symmetrically bound heavy-atom positions. A FORTRAN routine was written to consider all possible combinations of the two Pt and the two Hg sites within the estimated dimer diameter of each other and related by the molecular dyad axis. The position and orientation of the dimer axis was refined against the dimer electron density. The molecular mask was generated from skeletonized atoms created by the density-tracing routine in O [43] from a once-averaged MIR map. The solvent-protein boundary was clear in most places. The real-space correlation between dimer subunits within the molecular envelope in the initial 2.5 Å MIR map was 0.55. Phase improvement by solvent flattening and local twofold symmetry averaging was carried out with local AVGSYS programs (JT Bolin, JLS and SW Muchmore. Considerations in phase refinement and extension: experiments with a rapid and automatic procedure. Abstracts of the American Crystallographic Association Meeting 1993. Vol. 21, p. 51) implemented to use the fast Fourier transform routines of CCP4. The phase-refined 2.5 Å map had a dimer correlation of 0.83 and was easily interpreted.

Model building and refinement

Model building was done with skeletonized electron density by reference to a database of well refined structures using the graphics package O. One subunit was built into the phase refined 2.5 Å map, and the other subunit was generated with the dyad symmetry operator. Using stereochemical information, the initial model coordinates of the inactivator were generated using the program QUANTA3.3 (Molecular Simulations Inc., San Diego, CA). The geometric restraints for the covalently bound inactivator were defined based on related small molecule crystal structures in the Cambridge Structural Database. The model was refined with X-PLOR [44] with stereochemical target values and associated force constants based on a statistical analysis of the Cambridge Structural Database [45]. The two subunits of the dimer were refined independently of each other. The initial R-factor of 46% for

Table 3

Heavy-atom information.

Compound	Conc. (mM)	Soak time	No. of sites	Positions (unit cell fractions) x	y	z	Occupancy (arbit. scale)	B-factor (Å^2)
K_2PtCl_4	2.0	12 h	2	−0.2456	0.0104	0.3922	1.0	28
				−0.0647	0.0219	0.4502	0.67	29
$EthylHgPO_4$	0.01	10 days	2	0.1515	0.1578	0.0746	0.33	21
				−0.2940	0.1720	−0.0370	0.32	21

7.0–2.5 Å data decreased to 33% after minimization and dropped to 26% after one round of simulated annealing. The refinement consisted of two rounds of simulated annealing and six rounds of least-squares minimization, with manual adjustment and addition of waters to the protein model at each round. Data to 2.0 Å were added after the third round of refinement. Water molecules were selected from F_o–F_c density peaks by analysis of their distances to hydrogen-bond donors or acceptors of the protein or to other waters (local program PEAKCHECK by JLS). The individual occupancies of the water molecules were assigned based on a linear scale of the electron density peak heights, with the highest peak given a value of 1.0 and the lowest given a value of 0.4. Individual isotropic temperature factors for water molecules were refined; occupancies were not. Refinement was terminated when the majority of the largest peaks in the F_o–F_c map could not be accounted for by additional solvent or adjustments to the protein model.

Two aspects of the model that demanded special caution against bias were the bound inactivator moiety with its many degrees of torsional freedom, and two non-proline cis-peptides in each polypeptide. As the two subunits of the dimer were refined independently, different methods of model building were used in the two subunits to minimize bias. The inactivator of one subunit was built into the initial density. In the other subunit we attempted to develop a less biased image of the inactivator. For a few rounds of refinement, additional water molecules were placed into the inactivator electron density at maxima in the F_o–F_c map as 'dummy' atoms free of bond restraints. When the number of dummy atoms reached approximately half the number of inactivator atoms, the inactivator model was built, based on the dummy-atom positions. The two refined models agreed to within experimental error. The certainty of the non-proline *cis*-peptides was also tested through independent refinement in the two subunits as *cis* and *trans*. Characteristic F_o–F_c difference peaks and disallowed main-chain torsion angles for the second residue of each *cis*-peptide were consistently observed when the peptide was modelled and refined in the *trans* conformation. Nine cases of multiple conformations for main-chain or side-chain groups were also observed during the course of refinement. The multiple conformers were not refined simultaneously.

Structure determination of free dehydrase involved refinement of the inactivated enzyme model against the free dehydrase data. All refinement was carried out with X-PLOR. The starting model consisted of the two polypeptide chains of the dimer without the inactivator or solvent molecules. In trial rounds of rigid body and atomic refinement, the *cis*-peptide segment His70–Phe71 was also omitted from the model, in the expectation that the *cis*-peptide in the inactivated structure was induced by covalent modification of His70. However, electron density of the omitted segment was clearly that of a *cis*-peptide in the free enzyme. Rigid-body refinement of the complete dimer against the data for the free enzyme (7–2.5 Å) decreased the initial R-factor of 38% to 28%. After further minimization, data to 2.0 Å were utilized. Water molecules were added in the same manner as for the inactivated structure.

Statistics for the inactivated and free dehydrase models are reported in Table 1. Geometric analysis of the model was with PROCHECK [46] and with options in X-PLOR and in O. Sequence comparisons to other proteins were carried out with BLAST [47] and CLUSTAL W [48]. Calculation of accessible surfaces was done with the program GRASP [49]. Atomic models are available from the Protein Data Bank with access codes of 1MKA for the inactivated enzyme and IMKB for the free enzyme.

Acknowledgements

We thank VJ Davisson (Purdue) for his suggestions with regard to the enzyme mechanism. Financial support was provided by the NIH (R01 GM36286 to JMS.) and from the NSF (8917132-DMB to JLS). X-ray facilities were supported in part by a grant from the Lucille P Markey Foundation.

References

1. Bloch, K. (1971). β-Hydroxydecanoyl thioester dehydrase. In *The Enzymes*. vol. **5**, pp. 441–464, .
2. Schwab, J.M. & Henderson, B.S. (1990). Enzyme-catalyzed allylic rearrangements. *Chem. Rev.* **90**, 1203–1245.
3. Helmkamp, G.M., Jr. & Bloch, K. (1969). β-Hydroxydecanoyl thioester dehydrase: studies on molecular structure and active site. *J. Biol. Chem.* **244**, 6014–6022.
4. Schwab, J.M. & Klassen, J.B. (1984). Steric course of the allylic rearrangement catalyzed by β-hydroxydecanoyl thioester dehydrase: mechanistic implications. *J. Am. Chem. Soc.* **106**, 7217–7227.
5. Brock, D.J.H., Kass, L.R. & Bloch, K. (1967). β-Hydroxydecanoyl thioester dehydrase. II. Mode of action. *J. Biol. Chem.* **242**, 4432–4440.
6. Helmkamp, G.M., Rando, R.R., Brock, D.J.H. & Bloch, K. (1968). β-Hydroxydecanoyl thioester dehydrase. Specificity of substrates and acetylenic inhibitors. *J. Biol. Chem.* **243**, 3229–3231.
7. Dessen, A., Quémard, A., Blanchard, J.S., Jacobs, W.R., Jr. & Sacchettini, J.C. (1995). Crystal structure and function of the isoniazid target of *Mycobacterium tuberculosis*. *Science* **267**, 1638–1641.
8 Rafferty, J.B., *et al.*, & Rice, D.W. (1995). Common themes in redox chemistry emerge from the X-ray structure of oilseed rape (*Brassica napus*) enoyl acyl carrier protein reductase. *Structure* **3**, 927–938.
9. Cronan, J.E., Li, W.-B., Coleman, R., Narasimhan, M., de Mendoza, D. & Schwab, J.M. (1988). Derived amino acid sequence and identification of active site residues of *Escherichia coli* β-hydroxydecanoyl thioester dehydrase. *J. Biol. Chem.* **263**, 4641–4646.
10. Annand, R.R., Kozlowski, J.F., Davisson, V.J. & Schwab, J.M. (1993). Mechanism-based inactivation of *Escherichia coli* β-hydroxydecanoyl thioester dehydrase: assignment of the imidazole ^{15}N NMR resonances and determination of the structure of the alkylated histidine. *J. Am. Chem. Soc.* **115**, 1088–1094.
11. Schwab, J.M., Ho, C.-K., Li, W.-B., Townsend, C.A. & Salituro, G.M. (1986). β-Hydroxydecanoyl thioester dehydrase. Complete characterization of the fate of the "suicide" substrate 3-decynoyl-NAC. *J. Am. Chem. Soc.* **108**, 5309–5316.
12. Schwab, J.M., Li, W.-B., Ho, C.-K., Townsend, C.A. & Salituro, G.M. (1984). Direct observation by carbon-13 NMR spectroscopy of the regioselectivity and stoichiometry of "suicide" enzyme inactivation. *J. Am. Chem. Soc.* **106**, 7293–7294.
13. Lundqvist, T., Rice, J., Hodge, C.N., Basarab, G.S., Pierce, J. & Lindqvist, Y. (1994). Crystal structure of scytalone dehydratase – a disease determinant of the rice pathogen, *Magnaporthe grisea*. *Structure* **2**, 937–944.
14. Coleman, J. & Raetz, C.R.H. (1988). First committed step of lipid A biosynthesis in *E. coli*: sequence of the *lpxA* gene. *J. Bacteriol.* **170**, 1268–1274.

15. Mohan, S., Kelly, T.M., Eveland, S.S., Raetz, C.R.H. & Anderson, M.S. (1994). An *Escherichia coli* gene (*FabZ*) encoding (*3R*)-hydroxymyristoyl acyl carrier protein dehydrase. *J. Biol. Chem.* **269**, 32896–32903.
16. Silverman, R. (1988). *Mechanism-Based Enzyme Inactivation: Chemistry and Enzymology*. Vol. 1, CRC Press, Boca Raton, FL.
17. Rando, R.R. & Bloch, K. (1968). Mechanism of action of β-hydroxydecanoyl thioester dehydrase. *J. Biol. Chem.* **243**, 5627–5634.
18. Endo, K., Helmkamp, G.M., Jr. & Bloch, K. (1970). Mode of inhibition of β-hydroxydecanoyl thioester dehydrase by 3-decynoyl-*N*-acetylcysteamine. *J. Biol. Chem.* **245**, 4293–4296.
19. Gerlt, J.A. & Gassman, P.G. (1993). Understanding the rates of certain enzyme-catalyzed reactions: proton abstraction from carbon acids, acyl-transfer reactions, and displacement reactions of phosphodiesters. *Biochemistry* **32**, 11943–11952.
20. Cleland, W.W. & Kreevoy, M.M. (1994). Low-barrier hydrogen bonds and enzymic catalysis. *Science* **264**, 1887–1890.
21. Guthrie, J.P. & Kluger, R. (1993). Electrostatic stabilization can explain the unexpected acidity of carbon acids in enzyme-catalyzed reactions. *J. Am. Chem. Soc.* **115**, 11569–11572.
22. Brown, J.H., *et al.*, & Wiley, D.C. (1993). Three-dimensional structure of the human class II histocompatibility antigen HLA-DR1. *Nature* **364**, 33–39.
23. Valegard, K., Liljas, L., Fridborg, K. & Unge, T. (1990). The three-dimensional structure of the bacterial virus MS2. *Nature* **345**, 36–41.
24. Lawrence, C.M., Rodwell, V.W. & Stauffacher, C.V. (1995). Crystal structure of *Pseudomonas mevalonii* HMG-CoA reductase at 3.0 angstrom resolution. *Science* **268**, 1758–1762.
25. Henderson, B.S. (1992). Inactivation of β-hydroxydecanoyl thiol ester dehydrase by a photoreactive mechanism-based inactivator [PhD Thesis]. Purdue University, West Lafayette, IN.
26. Stein, J.P., Jr. (1976). Studies of the active site of β-hydroxydecanoyl thioester dehydrase from *Escherichia coli* [PhD Thesis]. Harvard University, Cambridge, MA.
27. Herzberg, O. & Moult, J. (1991). Analysis of the steric strain in the polypeptide backbone of protein molecules. *Proteins* **11**, 223–229.
28. Hanson, K.R. & Rose, I.A. (1975). Interpretation of enzyme reaction stereospecificity. *Accounts Chem. Res.* **8**, 1–10.
29. Schwab, J.M., Habib, A. & Klassen, J.B. (1986). A thorough study of the stereochemical consequences of the hydration/dehydration reaction catalyzed by β-hydroxydecanoyl thioester dehydrase. *J. Am. Chem. Soc.* **108**, 5304–5308.
30. Kass, L.R., Brock, D.J.H. & Bloch, K. (1967). β-Hydroxydecanoyl thioester dehydrase: I. Purification and properties. *J. Biol. Chem.* **242**, 4418–4431.
31. Guerra, D.J. & Browse, J.A. (1990). *Escherichia coli* β-hydroxydecanoyl thioester dehydrase reacts with native C_{10} acyl-acyl- carrier proteins of plant and bacterial origin. *Arch. Biochem. Biophys.* **280**, 336–345.
32. Holak, T.A., Kearsley, S.K., Kim, Y. & Prestegard, J.H. (1988). Three-dimensional structure of acyl carrier protein determined by NMR pseudoenergy and distance geometry calculations. *Biochemistry* **27**, 6135–6142.
33. Kim, Y. & Prestegard, J.H. (1989). A dynamic model for the structure of acyl carrier protein in solution. *Biochemistry* **28**, 8792–8797.
34. Annand, R.R. (1992). Studies on the fate of *S*-(3-decynoyl)-*N*-acetylcysteamine in *Escherichia coli* [PhD Thesis]. Purdue University, West Lafayette, IN.
35. Kass, L.R. (1969). β-Hydroxydecanoyl thioester dehydrase from *Escherichia coli*. *Methods Enzymol.* **14**, 73–80.
36. Sharma, A., Henderson, B.S., Schwab, J.M. & Smith, J.L. (1990). Crystallization and preliminary X-ray analysis of β-hydroxydecanoyl thiol ester dehydrase from *Escherichia coli*. *J. Biol. Chem.* **265**, 5110–5112.
37. Kabsch, W. (1988). Evaluation of single-crystal X-ray diffraction data from a position-sensitive detector. *J. Appl. Cryst.* **21**, 916–924.
38. Collaborative Computational Project No. 4. (1994). The CCP4 suite: programs for protein crystallography. *Acta Cryst. D* **50**, 760–763.
39. Otwinowski, Z. (1993). Oscillation data reduction program. In *Data Collection and Processing*. (Sawyer, .L., Issacs, N. & Bailey, S., eds), pp. 56–62, SERC Daresbury Laboratory, Warrington, UK.
40. Terwilliger, T.C. & Eisenberg, D. (1983). Unbiased three-dimensional refinement of heavy-atom parameters by correlation of origin-removed Patterson functions. *Acta Cryst. A* **39**, 813–817.
41. Otwinowski, Z. (1991). Maximum likelihood refinement of heavy atom parameters. In *Isomorphous Replacement and Anomalous Scattering*. (Wolf, W., Evans, P.R. & Leslie, A.G.W., eds), pp. 80–86, SERC Daresbury Laboratory, Warrington, UK.
42. Tong, L. & Rossmann, M.G. (1990). The locked rotation function. *Acta Cryst. A* **46**, 783–792.
43. Jones, T.A., Zou, J.Y., Cowan, S.W. & Kjeldgaard, M. (1991). Improved methods for the building of protein models in electron density maps and the location of errors in these models. *Acta Cryst. A* **47**, 110–119.
44. Brünger, A.T. (1992). *X-PLOR Version 3.1. A system for X-ray Crystallography and NMR*. vol. **382**. Yale University Press, New Haven and London.
45. Engh, R.A. & Huber, R. (1991). Accurate bond and angle parameters for X-ray protein structure refinement. *Acta Cryst. A* **47**, 392–400.
46. Laskowski, R.A., MacArthur, M.W., Moss, D.S. & Thornton, J.M. (1993). PROCHECK: a program to check the stereochemical quality of protein structures. *J. Appl. Cryst.* **26**, 283–291.
47. Altschul, S.F., Gish, W., Miller, W., Myers, E.W. & Lipman, D.J. (1990). Basic local alignment search tool. *J. Mol. Biol.* **215**, 403–410.
48. Thompson, J.D., Higgins, D.G. & Gibson, T.J. (1994). CLUSTAL W: improving the sensitivity of progressive multiple sequence alignment through sequence weighting, position specific gap penalties and weight matrix choice. *Nucleic Acids Res.* **22**, 4673–4680.
49. Nicholls, A., Sharp, K.A. & Honig, B. (1991). Protein folding and association: insights from the interfacial and thermodynamic properties of hydrocarbons. *Proteins* **11**, 281–296.
50. Engelman, D.M., Steitz, T.A. & Goldman, A. (1986). Identifying nonpolar transbilayer helices in amino acid sequences of membrane proteins. *Annu. Rev. Biophys. Biophys. Chem.* **15**, 321–353.